PERGAMON

International Journal of Heat and Mass Transfer 42 (1999) 49–59

International Journal of HEAT and MASS TRANSFER

Large-eddy simulation of turbulent flow over a two-dimensional cavity with temperature fluctuations

Arlindo de Matos, Francisco A. A. Pinho, Aristeu Silveira-Neto*

Federal University of Uberlândia, Department of Mechanical Engineering, 380440-206-Uberlândia-MG, Brazil

Received 23 January 1997; in final form 6 April 1998

Abstract

Large-eddy simulation of turbulent flow over a plane free cavity and over a plane symmetric cavity was performed. The Smagorinsky sub-grid scale turbulence model was used. The compressible formulation and the MacComarck finite volume method were employed. The dynamic and thermal behavior of a thermal capacitor were analyzed. This behavior presents strong dependence on the geometry and the temperature fluctuation frequency which is imposed in the entrance of capacitor and a little dependence on the Reynolds Number.

Nomenclature

C_S Smagorinsky constant
e_t total energy
f frequency
$\vec{g}$ gravity acceleration
$\vec{i}$ unitary vector in the x direction
$\vec{j}$ unitary vector in the y direction
k_c cutoff wave number
l sub-grid characteristic length ($l = \sqrt{\Delta x \Delta y}$)
M Mach number
p pressure
Pr Prandtl number
$\vec{q}$ conductive heat transfer
Re Reynolds number
S_{ij} deformation tensor
t non dimensional time
u velocity component in the x direction
U average velocity at the inlet of the cavity
v velocity component in the y direction
Δx grid dimension in the x direction
Δy grid dimension in the y direction
Δt time step.

Greek symbols
α molecular thermal diffusion
δ_{ij} Kronecker delta
κ molecular thermal conductivity
κ_t turbulent thermal conductivity
μ molecular dynamic viscosity
μ_t turbulent dynamic viscosity
ρ density
$\bar{\bar{\tau}}$ viscous stress tensor.

Subscripts
$()_{ij}$ tensor notation
t turbulent property
x Cartesian coordinate
y Cartesian coordinate
∞ reference property.

Acronym
LES Large-Eddy Simulation.

1. Introduction

Turbulent flow has been of interest to many researchers due to the practical implications and due to the fascinating phenomena intrinsic to fluid motion encountered in nature. A great advance in the comprehension of this kind of problem was attained in the last two decades due to the advance in the experimental methods, instrumentation and electronic acquisition systems and due to the spectacular advances in the numerical methods and the computational resources. A large energy spectrum is one of the most important physical characteristics of

* Corresponding author.

0017–9310/98 $19.00
PII: S0017–9310(98)00155–0

turbulent flows. The immediate consequence is that it is very difficult to simulate all scales that characterize a turbulent flow, i.e., to make the so-called direct numerical simulation. The current generation of computers allows direct simulation only for flows of low Reynolds numbers. However, the large majority of practical and natural turbulent flows are characterized by a large Reynolds number.

The classical modeling methods consider the average behavior of the flow and calculate all scales of the spectra statistically. An intermediate method consists to solve part of the flow, the bigger vortices or the small wave numbers, and to model the small vortices or the high wave numbers. The cutoff wave number ($k_c = 2\pi/l$) is determined by the grid dimension ($l = \sqrt{\Delta x \Delta y}$). This method, known as Large-Eddy Simulation (LES), was developed by Smagorinsky [1] and has been largely used in recent years. So-called sub-grid scale models are used to model the high wave numbers. The Smagorinsky [1] eddy viscosity model is one used most frequently and becomes very popular after the pioneering engineering work of Deardorff [2] for a channel flow. This basic model has given origin to a family of derived models [3]. The most important recent development is the dynamic model proposed by Germano et al. [4].

Another family of sub-grid scale models is based on the Kraichnan spectral eddy viscosity theory. A practical and frequently used version of this family of models was developed by [5], the structure function model, and was used in several LES works [6, 7]. This model has the important characteristic that the only constant involved is determined analytically. The constant of the Smagorinsky model is adjusted and depends on some parameter like the discretization grid. In the present work the Smagorinsky model was used to develop LES of turbulent flow over a two-dimensional cavity with temperature fluctuations. The structure function model is restrained to three-dimensional simulations.

Turbulent flows are basically three-dimensional, but some kinds of flows can be treated approximately with a two-dimensional hypothesis. In the present case the flow is transitioning and the dynamic instabilities are not completely three-dimensional. So, due to the computational resource limitations, the two-dimensional approximation is used here.

The objective of the present work is to analyze numerically the physical phenomena involved in the damping process of temperature fluctuations that occurs in the interior of a two-dimensional cavity. This kind of equipment is normally placed in a tubing system in order to promote the damping of undesirable thermal or dynamic fluctuations that appear in many practical applications. The comprehension of the physical phenomena involved in this problem is very important to design better this kind of device. This understanding requires the visualization of the temperature fluctuations and its transport by the flow. LES is very appropriate for this, because it is possible to simulate the dynamic and thermal instabilities involved in the turbulent flow.

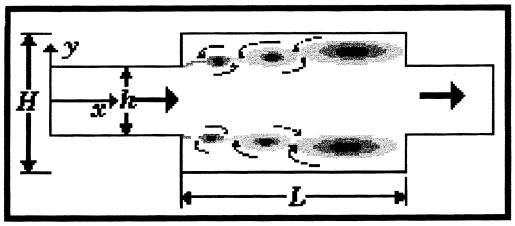

Fig. 1. Plane symmetric cavity, geometric and physic characteristics.

Basic physical and geometrical characteristics of the problem are illustrated in Fig. 1. The coherent structures that must be shed in the expansion of the cavity as a consequence of the mean shear flow generated by the circulation are shown qualitatively. These structures are very important in the process of mixing the flow properties and accelerate the damping process of temperature fluctuations in the cavity. In the next section the mathematical model is presented.

2. Mathematical model

The mass, momentum and energy non-dimensional equations are considered for compressible two-dimensional flow of Newtonian fluids. These equations can be written, after a filtering process that characterize a large-eddy simulation [6], in generalized fashion as follows:

$$\frac{\partial \vec{\vec{U}}}{\partial t} + \nabla \cdot \vec{\vec{P}} = \vec{\vec{G}} \tag{1}$$

where

$$\vec{\vec{U}} = \begin{bmatrix} [\rho] \\ [\rho]\bar{u} \\ [\rho]\bar{v} \\ [\rho]\bar{e}_t \end{bmatrix}, \tag{2}$$

$$\vec{\vec{P}} = \vec{\vec{E}} \otimes \vec{i} + \vec{\vec{F}} \otimes \vec{j}, \tag{3}$$

$$\vec{\vec{E}} = \begin{bmatrix} [\rho]\bar{u} \\ [\rho]\bar{u}\bar{u} + \bar{p} - \bar{\tau}_{xx} \\ [\rho]\bar{u}\bar{v} - \bar{\tau}_{xy} \\ ([\rho]\bar{e}_t + \bar{p})\bar{u} - \bar{u}\bar{\tau}_{xx} - \bar{v}\bar{\tau}_{xy} + \bar{q}_x \end{bmatrix} \tag{4}$$

$$\vec{\vec{F}} = \begin{bmatrix} [\rho]\bar{v} \\ [\rho]\bar{v}\bar{u} - \bar{\tau}_{yx} \\ [\rho]\bar{v}\bar{v} + \bar{p} - \bar{\tau}_{yy} \\ ([\rho]\bar{e}_t + \bar{p})\bar{v} - \bar{u}\bar{\tau}_{yx} - \bar{v}\bar{\tau}_{yy} + \bar{q}_y \end{bmatrix} \tag{5}$$

$$\vec{\bar{G}} = \begin{bmatrix} 0 \\ [\rho]g_x \\ [\rho]g_y \\ \bar{u}g_x + \bar{v}g_y \end{bmatrix}, \tag{6}$$

$$\bar{\tau}_{ij} = \tfrac{2}{3}\frac{(\mu+\mu_t)}{Re}\bar{S}_{ij} - \delta_{ij}\frac{\partial \bar{u}_k}{\partial x_k}, \tag{7}$$

$$\bar{q}_j = -\frac{(k+k_t)}{(\gamma-1)M^2 Re\, Pr}\frac{\partial \bar{T}}{\partial x_j}. \tag{8}$$

The following state equations of the fluid were used:

$$\bar{p} = (\gamma-1)[\rho]\bar{e}_i, \tag{9}$$

$$\mu = \frac{C_1 \bar{T}^{3/2}}{C_2 + \bar{T}}, \tag{10}$$

$$\bar{T} = \frac{\gamma M^2_{\infty]}\bar{p}}{[\rho]}, \tag{11}$$

where $C_1 = 1.458 \times 10^{-6}$, $C_2 = 110.4$, $\gamma = 1.4$, and V_∞ and M_∞ are respectively the velocity and the Mach number at the reference state.

These equations were filtered in order to separate the large scales and the sub-grid scales of the turbulent flow. The $(^-)$ that appears over all variables in these equations represents this filtration process. This filter process gives rise to additional stress tensors like the sub-grid scale Reynolds tensor, the Leonard tensor and the crossed tensor. The sub-grid Reynolds tensor was modeled using the classical Boussinesq hypotheses, equation (7). The two other tensors were neglected as a consequence of the order of precision of the transport scheme used in this work (second order). As verified by Silveira-neto et al. [6], if the scheme is up to a third order, the Leonard and the crossed tensor are negligible as compared with the sub-grid Reynolds Stress.

The sub-grid turbulent viscosity μ_i and thermal diffusion coefficient κ_i are calculated with the Smagorinsky [1] model and with the hypothesis of the turbulent Prandtl number, given by:

$$v_t = (C_s l)^2\sqrt{2\bar{S}_{ij}\bar{S}_{ij}}, \tag{12}$$

$$\alpha_t = \frac{v_t}{Pr_t}, \tag{13}$$

$$\bar{S}_{ij} = \tfrac{1}{2}\left(\frac{\partial \bar{u}_i}{\partial x_j} + \frac{\partial u_j}{\partial x_i}\right), \tag{14}$$

where $l = \sqrt{\Delta x \Delta y}$ is the characteristic length, Δx and Δy are the discretization grid intervals and C_s the Smagorinsky constant, adjusted in this work to be 0.4 [8]. We have taken $Pr_t = 0.6$ [6].

The Smagorinsky model depends only on the deformation ratio and can introduce artificial turbulent viscosity in the laminar portion of the flow. It can be corrected using a selective Smagorinsky model, which is in development by the authors.

3. Numerical method

The MacComarck [10] finite volume method was used in order to make the discretization of the differential equations described above [9].

After the integration of equation (1), we have the following resultant equations:

Predictor step:

$$\Delta\vec{U}^{\overline{n+1}}_{i,j} = -\frac{\Delta t}{V_{ij}}\left(\begin{matrix}\vec{\bar{P}}_{i+1j}\vec{S}_{i+1/2j} - \vec{\bar{P}}_{ij}\vec{S}_{i-1/2j} \\ + \\ \vec{\bar{P}}_{ij+1}\vec{S}_{ij+1/2} - \vec{\bar{P}}_{ij}\vec{S}_{ij-1/2}\end{matrix}\right)^n + \Delta t\vec{G}^n_{ij}, \tag{15}$$

$$\vec{U}^{\overline{n+1}}_{ij} = \vec{U}^n_{ij} + \Delta\vec{U}^{\overline{n+1}}_{ij}; \tag{16}$$

Corrector step:

$$\Delta\vec{U}^{n+1}_{ij} = -\frac{\Delta t}{V_{ij}}\left(\begin{matrix}\vec{\bar{P}}^{\overline{n+1}}_{ij}\vec{S}_{i+1/2j} - \vec{\bar{P}}^{\overline{n+1}}_{i-1j}\vec{S}_{i-1/2j} \\ + \\ \vec{\bar{P}}^{\overline{n+1}}_{ij}\vec{S}_{ij+1/2} - \vec{\bar{P}}^{\overline{n+1}}_{ij-1}\vec{S}_{ij-1/2}\end{matrix}\right)^n + \Delta t\vec{G}^n_{ij} \tag{17}$$

$$\vec{U}^{n+1}_{ij} = \vec{U}^n_{ij} + \frac{(\Delta\vec{U}^{\overline{n+1}}_{ij} + \Delta\vec{U}^{n+1}_{ij})}{2}. \tag{18}$$

The $(\ )^n$ indicates previous time and $(\ )^{n+1}$ the current time. The boundary conditions used are the following:

over the solid walls the velocity in a virtual grid is imposed equal to the value of the velocity in the first grid in the interior of the domain, with opposite sign;
at the inlet of the domain a parabolic velocity profile is imposed;
at the outlet a developed flow is considered;
the walls are considered adiabatic and the temperature is imposed at the inlet and finally the pressure is extrapolated at the inlet of the domain.

The calculations were performed with the following mesh: 20×32 points in the inlet channel, 80×160 points in the cavity and 20×52 in the outlet channel. These points refer respectively to the x and y directions. This regular mesh ensures a size of 4.75×10^{-4} m in all domain. This mesh is not enough to describe all scales of the flow in the vicinity of the wall. In the present work the global flow structure, like the Kelvin and Helmholtz instabilities and the recirculation, govern the mixing process and the attenuation of temperature fluctuations. On the other hand an adiabatic boundary condition has been used and the heat transfer to the wall is zero. So, the simulation of all scales of the boundary layer seems to have a secondary importance in the global behavior of the system.

The calculations were performed at a PC 486DX4 and a Pentium 100 MHz. Each simulation presented took about 24 h of CPU time.

4. Results

The results presented are related to two kinds of cavities: the first is an open cavity without temperature fluctuations [8]. The second is a plane symmetric cavity with temperature fluctuations imposed at its inlet as illustrated in Fig. 1 [11].

4.1. Open cavity

In this case the upper side of the cavity is considered as a free flow and a velocity zero gradient was imposed ($\partial u/\partial y = 0$). These results are shown in Figs 2 and 3 for validation of the numerical code used in the second part of the work. Figure 2 shows the pressure coefficient, here defined as

$$C_p = \frac{2(p-p_\infty)}{\rho U_\infty^2},$$

where ∞ is the reference state, located at the free stream over the cavity. The result of the present calculation is in good agreement with the experimental result of Sinha and Oberai [12]. On the right hand side of the cavity there is an important difference, which may be due to the large uncertainty of the experimental data and also due to the numerical imprecision like the effect of the exit boundary conditions. More numerical simulations must be done to elucidate this point.

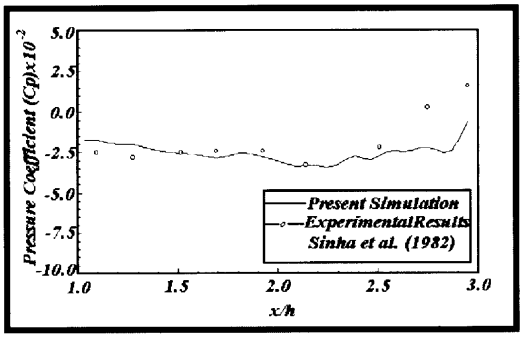

Fig. 2. Pressure coefficient; $Re = Uh/v = 2648$ (Reynolds number); $M = 0.005$ (Mach number); $L = 2\,h$.

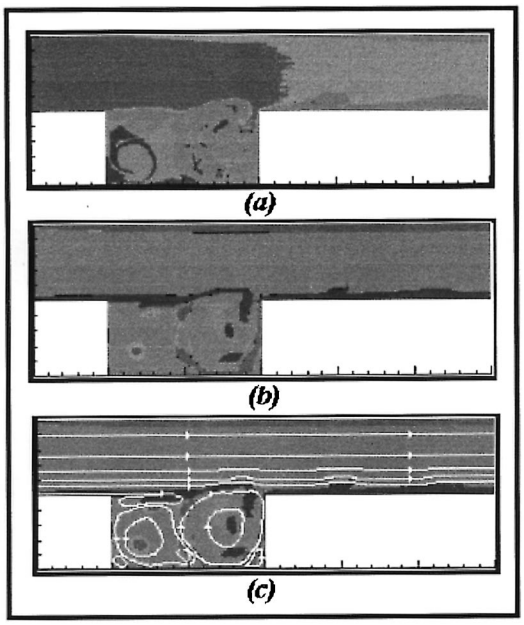

Fig. 3. Fields of density (a), vorticity (b) and stream lines (c); $Re = Uh/v = 2648$ (Reynolds number); $M = 0.005$ (Mach number); $L = 2\,h$.

In Fig. 3 the flow in the free cavity is shown in a regime statistically established. Figures 3a, b and c show respectively the density field, the vorticity field and the streamlines. There is a primary circulation in the clockwise sense generating another circulation in the counterclockwise sense. There are also four small circulations, generated by the primary and the secondary ones. This is in very good agreement with the experimental results of Sinha and Oberai [12]. It is interesting to note that the larger circulations are composed of a cluster of smaller vortices, as can be seen in Fig. 3c.

The numerical code used was originally developed by Miserda [13]. Several tests were performed with three-dimensional calculations. In the case of turbulent flow over a backward step it was found that the simulated reattachment length compares very well the experimental results of Eaton and Johnston [14], presenting an error of about 2%. Therefore, it was decided to use this computational code for the numerical experiments presented in the next section.

4.2. Plane symmetric cavity

In this section, the results of the numerical simulations of the flow over the plane symmetric cavity with temperature fluctuations imposed in the inlet of the channel are presented. In order to facilitate the presentation of results, the simulations realized are labeled as a function of the cavity geometry, the frequency of the temperature fluctuations and the Reynolds number, as shown in Table 1.

The results of simulation R30L01 are presented in Figs 4–8. Figure 4 shows the time evolution of the flow visualized with the vorticity fields. The time evolution of the dynamic instabilities is established. The periodical coherent vortices formed by the Kelvin–Helmholtz mechanisms [15] are visible. The turbulent structures have a characteristic length of the order of the step height. Hence it is difficult to transport them in the outlet of the cavity. They are constrained to circulate in the cavity and their energy is dissipated by the viscous effects. The cor-

Table 1
Key of simulations performed

Simulat.	$Re = Uh/v$	Length L	Freq.
R30L01	30 000	4 h	$0.1U/h$
R70L01	70 000	4 h	$0.1U/h$
R70L1	70 000	4 h	$1.0U/h$
R70C1	70 000	2 h	$1.0U/h$

responding temperature field is shown in Fig. 5. The temperature fluctuations imposed in the inlet have a frequency of $0.1U_\infty/h$ and an amplitude of 20 K over a mean value of 320 K, as shown in Fig. 6. In Fig. 5, the darker regions correspond to high temperatures and the lighter regions correspond to low temperatures. So, in Fig. 5 we see alternating dark and light packets of fluid that are injected in the entrance of the cavity. These packets are transported by convection towards the interior of the cavity, where they are adsorbed by diffusion. The result is shown in Fig. 7 where the outlet average (over y) temperature is plotted as a function of time. We see that the time average value is always 320 K but the amplitude is about 10 K. Hence, attenuation is about 50%. The Fourier transform of the time distribution of Fig. 7 is shown in Fig. 8. As expected, the principal frequency at the outlet is also $0.1U_\infty/h$. It is shown also that new harmonics were formed by the turbulent flow.

In order to investigate the Reynolds number influence we have performed the simulation R70L01. Figures 9–11 show the results. Figures 9 and 10 show similar vorticity and temperature fields as Figs 4 and 5 respectively. Figure 11 shows the time history of the outlet temperature which is also similar in amplitude to Fig. 7. The Fourier transform of this time distribution shows that the frequency $f = 0.1U/h$ also appears in the outlet of the cavity. This means that, at least in the range considered here, the Reynolds number does not affect the statistical result of temperature.

The influence of the frequency of the inlet temperature fluctuations has been analyzed by means of simulation R70L1. Figures 12–16 show the results. Figure 12 shows the flow dynamics by means of the time evolution of the vorticity fields. Comparing this figure with Fig. 9 (the same Reynolds number) we see that the flows are dynamically very similar. Nevertheless, comparing Fig. 13 with Fig. 10, we see that the thermal behavior is, as expected, completely different. The darker and light regions in Fig. 13 indicate the higher frequency of the inlet thermal fluctuations, as shown in Fig. 14. These temperature pulses are transported by convection and are quickly damped by the turbulent movement. Qualitatively, the damping process is more efficient when the inlet frequency is higher, see for example Fig. 13f and Fig. 10f. Figure 15

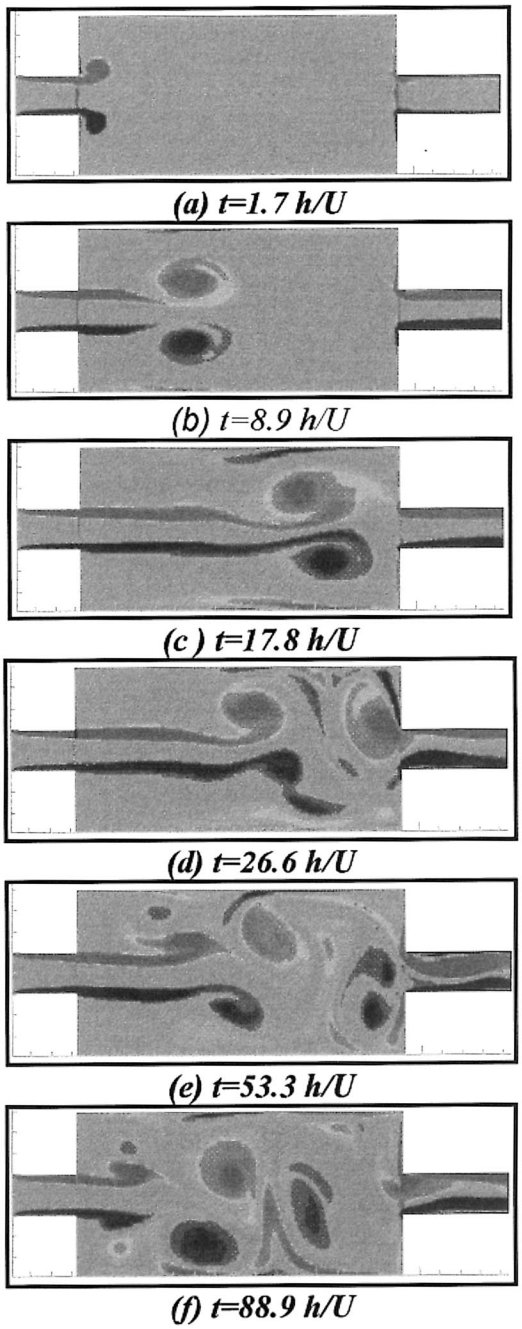

Fig. 4. Time evolution of the vorticity fields; run R30L01.

shows the temperature time history at the outlet of the cavity. We see that in the statistically established regime the amplitude of the temperature fluctuation is of order of 5 K, thus resulting in a damping of 88%. This confirms the previous conjectures: the damping process is much more efficient for the higher frequencies of the thermal fluctuations. Physically, the higher the entrance

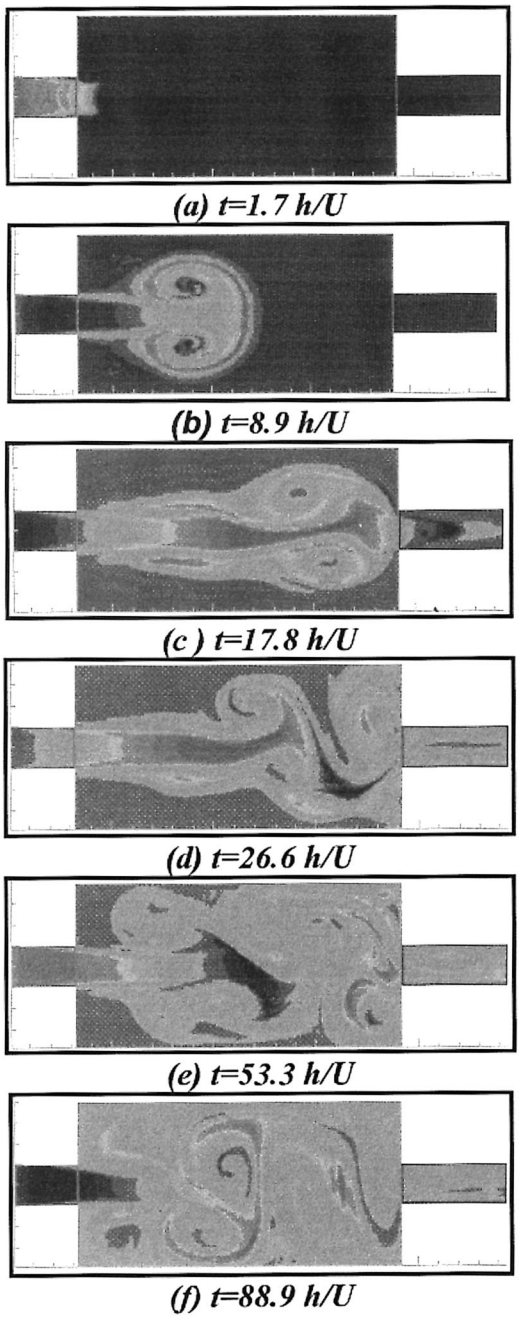

Fig. 5. Time evolution of the temperature fields; run R30L01.

frequency, the higher the temperature gradients in the interior of the cavity, accelerating the molecular diffusion. Figure 16 shows the Fourier transform of the outlet temperature distribution. We see that the inlet frequency of $1.0U/h$ is present at the outlet but with an intensity smaller than the intensity corresponding to the peak at $f = 0.05U/h$. Hence, the temperature distribution

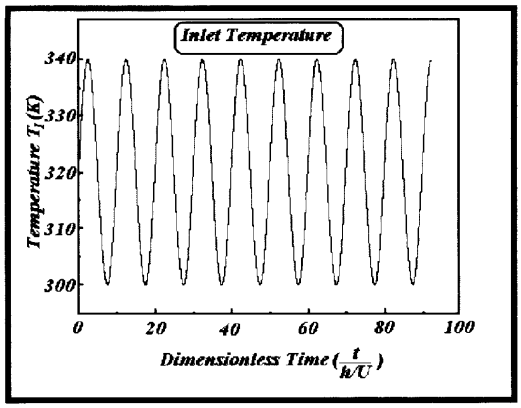

Fig. 6. Time history of the temperature at the inlet of the cavity; run R30L01.

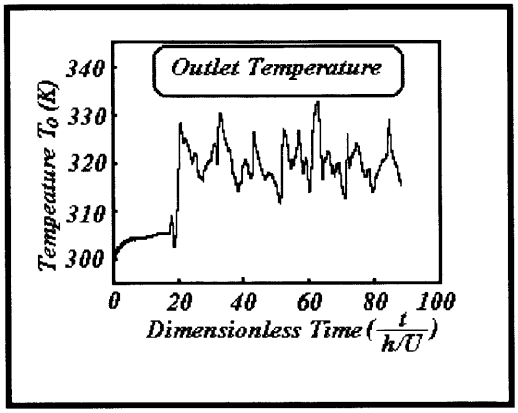

Fig. 7. Time history of the temperature at the outlet of the cavity; run R30L01.

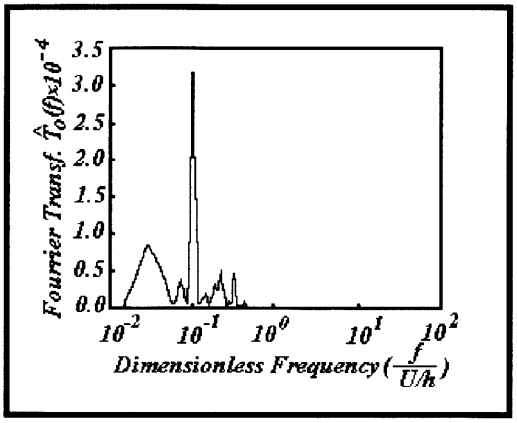

Fig. 8. Fourier transform of the outlet temperature; run R30L01.

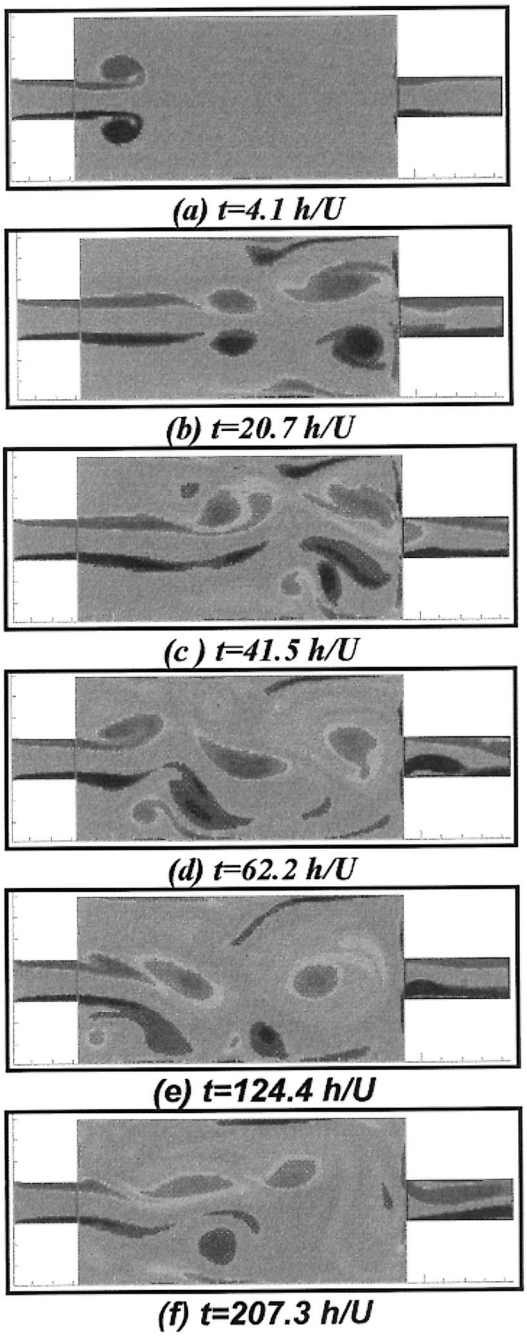

Fig. 9. Time evolution of the vorticity fields; run R70L01.

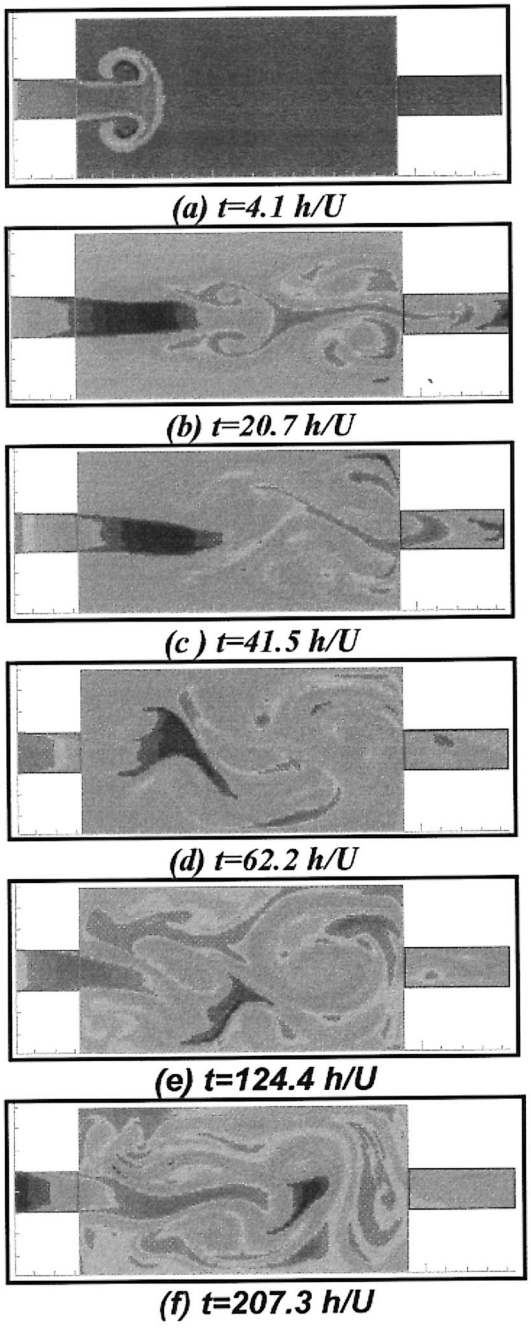

Fig. 10. Time evolution of the temperature fields; run R70L01.

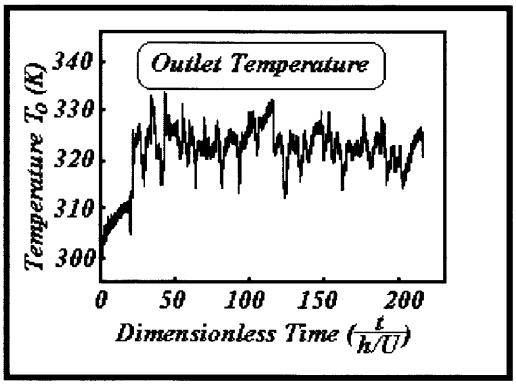

Fig. 11. Time distribution of the temperature at the outlet of the cavity; run R70L01.

at the outlet looses its coherence with the inlet distribution. This is a consequence of the strong damping occurring in the thermal capacitor in this run.

Finally, we have pointed out the dependency of the damping process on the geometry of the thermal capacitor. The simulation R70C1 was performed. Figure 17 shows, by means of the vorticity field, that the flow is more simple than the preceding ones. There are two symmetric circulations on the right hand side of the cavity such that the flow is very organized and forms a jet straight to the outlet. Figure 18 shows the corresponding temperature fields. We see again the alternating dark and light regions indicating a presence of fluctuating temperature at the inlet with a frequency of $1.0U/h$ as shown in Fig. 19. We see that the fluctuations are transported directly to the outlet without experiencing the circulation movement. However, Fig. 19 shows that the fluctuations were damped by about 67%. This is due to the high temperature gradients diffusing the thermal fluctuations as they are transported by convection. Compared to the previous results (R70L1, same parameters except the geometry) we see that the configuration with $L = 4\ h$ is more efficient than the configuration with $L = 2\ h$ because in the latter it is not possible to develop a turbulent flow. It may be possible to increase the damping process in the shorter capacitor by means of geometrical modifications like a shift of the outlet canal or a insertion of turbulence generators in the interior of the cavity. More simulations are required to analyze these kinds of modifications. It can be interesting also to study the pressure fluctuation damping.

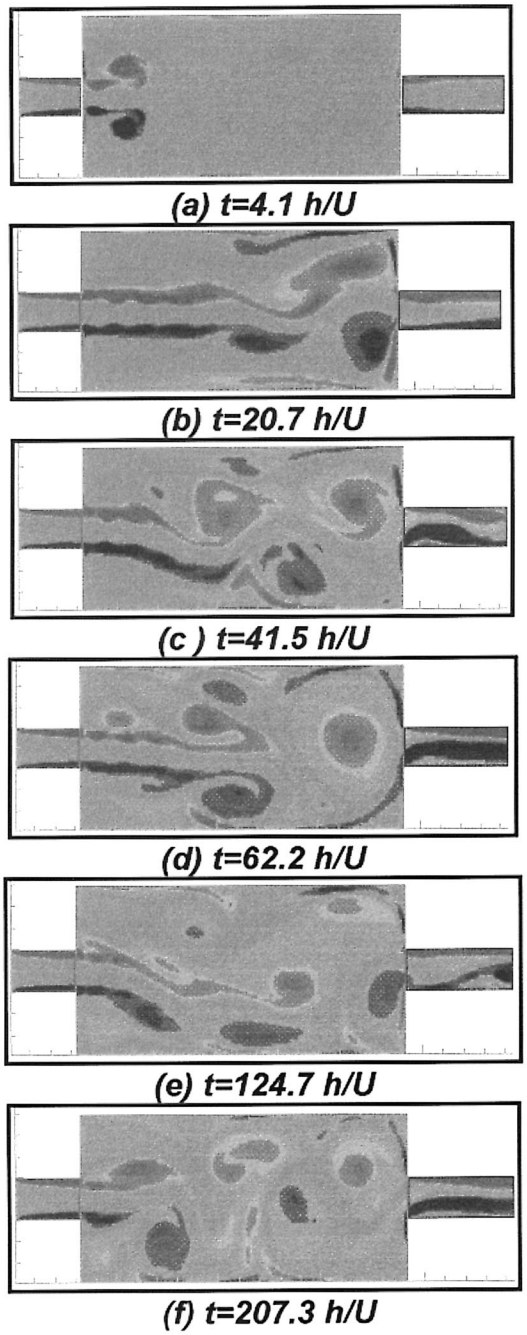

Fig. 12. Time evolution of the vorticity fields; run R70L1.

5. Conclusions

The dynamic and thermal behavior of a thermal capacitor was analyzed by Large-Eddy Simulation by means of a computational code based in a formulation for compressible flows. A sub-grid scale model gave stability to this numerical code for high Reynolds numbers.

The influence of three important parameters (Reynolds number, frequency of the fluctuations in the inlet of the cavity and the geometry) on the thermal fluctuation damping process was analyzed. The Reynolds number is

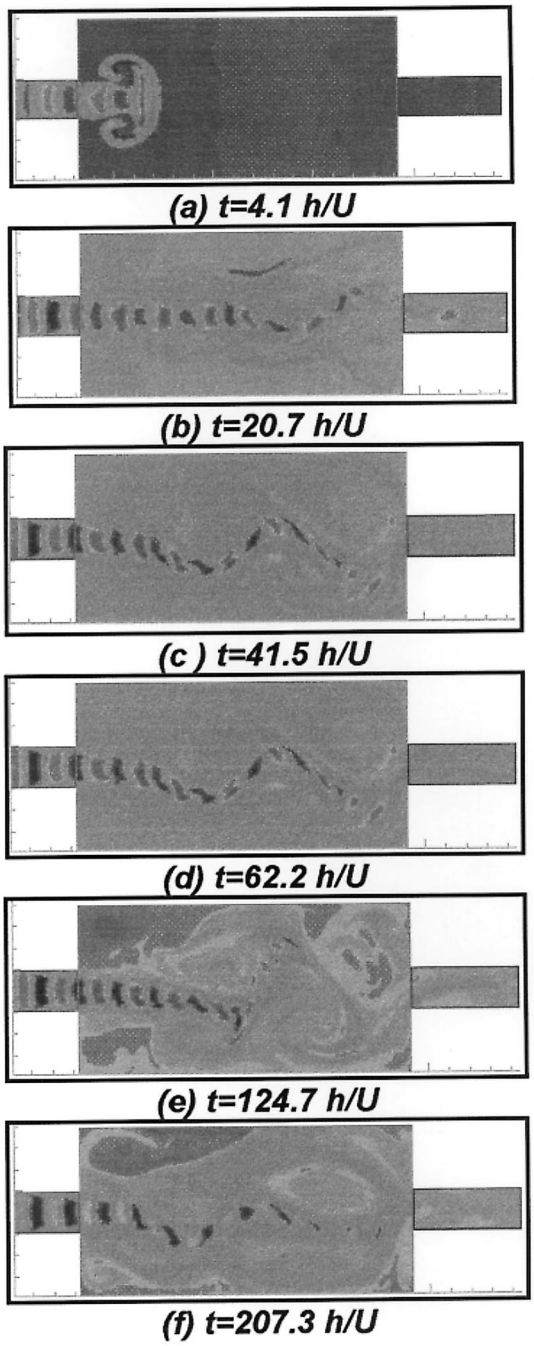

Fig. 13. Time evolution of the temperature fields; run R70L1.

not very important in the region between 30 000 and 70 000. It has been shown that the higher temperature frequencies are more efficiently damped than the lower frequencies. This is coherent with the physical argument that high frequencies create high local temperature gradients. The geometry is also very important and the

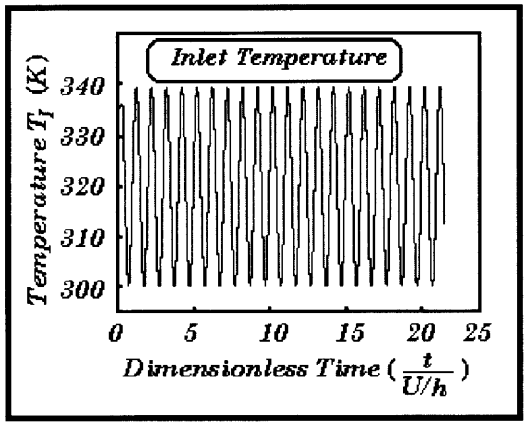

Fig. 14. Time history of the temperature at the inlet of the cavity; run R70L1.

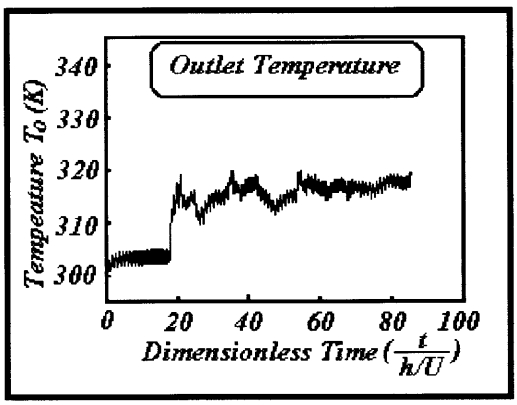

Fig. 15. Time history of the temperature at the outlet of the cavity; run R70L1.

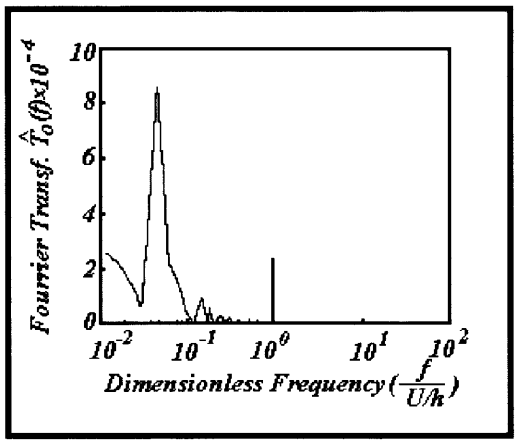

Fig. 16. Fourier transform of the outlet temperature; run R70L1.

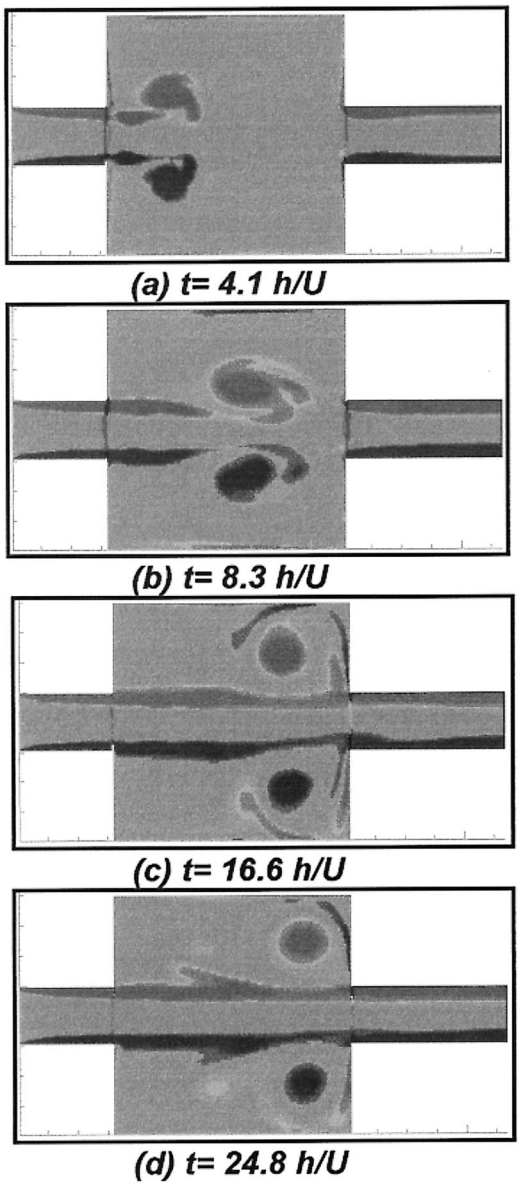

Fig. 17. Time evolution of the vorticity fields; run R70C1.

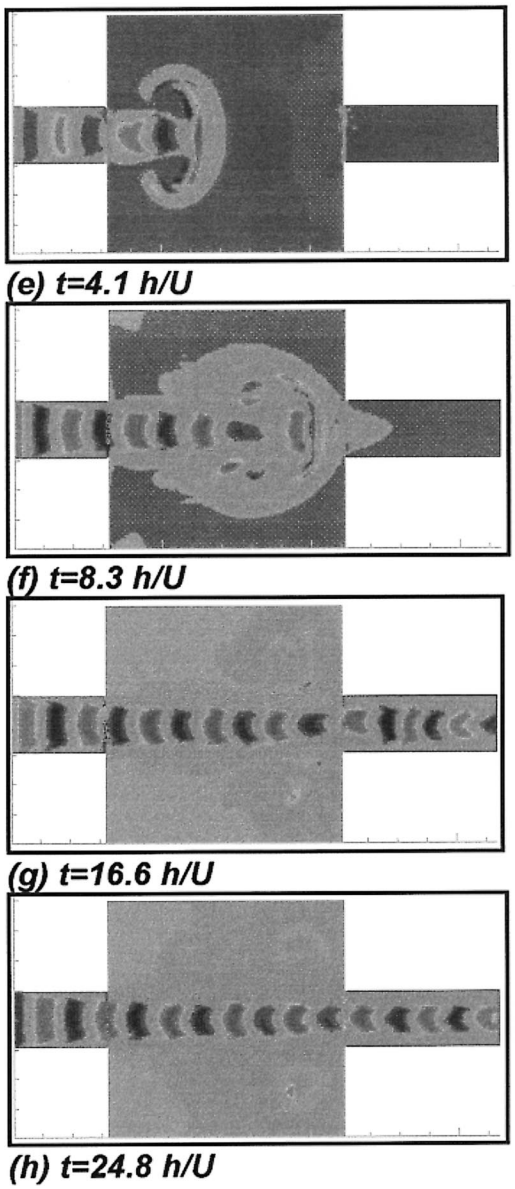

Fig. 18. Time evolution of the temperature at fields; run R70C1.

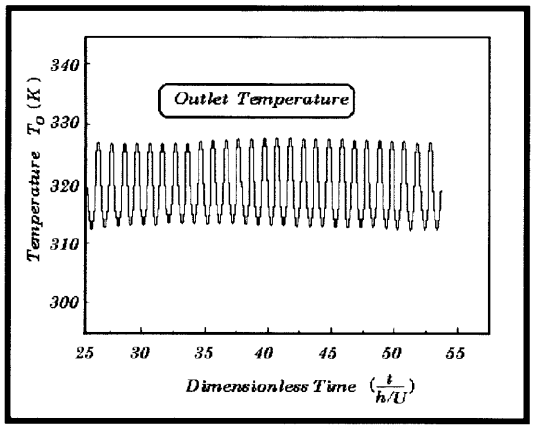

Fig. 19. Time history of the temperature at the outlet of the cavity; run R70C1.

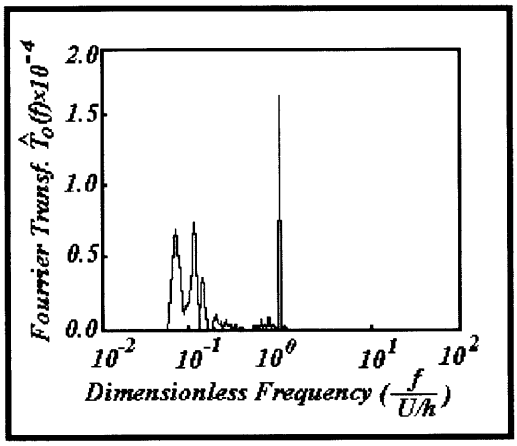

Fig. 20. Fourier transform of the outlet temperature; run R70C1.

designer must choose the relation L/h such that the turbulence intensity in the cavity is maximized.

Other geometrical parameters must be analyzed, like the shift of the axis of the outlet channel as compared with the axis of the inlet channel. Also, the presence of turbulence generators can be useful in order to increase the thermal damping process.

Acknowledgements

The authors are grateful to CNPq (Brazil) for financial support, to the post graduation course of Mechanical Engineering of the Federal University of Uberlândia and to Prof. Marc Mulkens for the English corrections.

References

[1] J. Smagorinsky, General circulation experiments with the primitive equations, Weather Rev. 91 (1963) 99–164.
[2] J.W. Deardorff, A numerical study of three-dimensional turbulent channel flow at large Reynolds number, J. Fluid Mech. 41 (1970) 453–480.
[3] P. Moin, J. Kim, Numerical investigation of turbulent channel flow, J Fluid Mech. 118 (1982) 341–377.
[4] M. Germano, U. Piomelli, P. Moin, W. Cabot, A dynamic subgrid-scale eddy-viscosity model, Phys Fluids A 3 (1991) 1760–1765.
[5] O. Métais, M. Lesieur, Spectral large eddy simulations of isotropic and stably-stratified turbulence, J. Fluid Mech. 239 (1992) 157–194.
[6] A. Silveira Neto, D. Grand, O, Métais, M. Lesieur, A numerical investigation of the coherent vortices in turbulence behind a backward-facing step, J. Fluid Mech. 256 (1993) 1–25.
[7] E. David, Modéelisation des écoulements compressibles et hypersoniques: une approche instationnaire. PhD thesis, Natl. Polytech. Inst., Grenoble, 1993.
[8] F.A.A. Pinho, Simulação numérica de grandes escalas de escoamentos turbulentos em cavidades retangulares bidimensionais, MSc dissertation, Federal University of Uberlândia, Brazil, 1995.
[9] D.A. Anderson, J.C. Tanehill, R.H. Pletcher, Computational Fluid Mechanics and Heat Transfer. Hemisphere Publishing Corporation, 1984.
[10] R.W. MacCormack, The effect of viscosity hypervelocity impact cratering. AIAA paper 1969, pp. 69–354.
[11] A. de Matos, Simulação numérica de grandes escalas de escoamentos turbulentos em cavidades retangulares axisimetricas, MSc dissertation, Federal University of Uberlândia, Brazil, 1996.
[12] S.N. Sinha, M.M. Oberai, Laminar separating flow over a backstep and cavity, Part II: Cavities. AIAA Journal 2 (1982) 370–375.
[13] R.B. Miserda, Simulação nume[faac]rica de grandes escalas de escoamentos turbulentos através de uma Formulação compressível para baixos números de Mach, PhD thesis, University of Brasilia, Brazil, 1996.
[14] J.K. Eaton, J.P. Johnston, Turbulent flow reattachment: an experimental study of flow structure behind backward-facing step. Stanford University, Report MD-39, 1980.
[15] M. Lesieur, Turbulence in Fluids. Kluwer Academic Publishers, 1990.